

Initial-state temperature of light meson emission source from squared momentum transfer spectra in high-energy collisions

Qi Wang^{1,*}, Fu-Hu Liu^{1,†}, Khusniddin K. Olimov^{2,‡}

¹*Institute of Theoretical Physics, State Key Laboratory of Quantum Optics and Quantum Optics Devices
& Collaborative Innovation Center of Extreme Optics, Shanxi University, Taiyuan 030006, China*

²*Laboratory of High Energy Physics, Physical-Technical Institute of Uzbekistan Academy of Sciences,
Chingiz Aytmatov str. 2^b, 100084 Tashkent, Uzbekistan*

Abstract: The squared momentum transfer spectra of light mesons, π^0 , π^+ , η , and ρ^0 , produced in high-energy virtual photon-proton (γ^*p) \rightarrow meson + nucleon process in electron-proton (ep) collisions measured by the CLAS Collaboration are analyzed by the Monte Carlo calculations, where the transfer undergoes from the incident γ^* to emitted meson or equivalently from the target proton to emitted nucleon. In the calculations, the Erlang distribution from a multi-source thermal model is used to describe the transverse momentum spectra of emitted particles. Our results show that the average transverse momentum ($\langle p_T \rangle$) and the initial-state temperature (T_i) increase from lower squared photon virtuality (Q^2) and Bjorken variable (x_B) to higher one. This renders that the excitation degree of emission source, which is described by $\langle p_T \rangle$ and T_i , increases with increasing of Q^2 and x_B .

Keywords: Initial-state temperature, average transverse momentum, squared momentum transfer, Erlang distribution

PACS numbers: 12.40.Ee, 14.40.-n, 24.10.Pa, 25.75.Ag

I. INTRODUCTION

In the evolution process of high-energy nucleus-nucleus (heavy-ion) collisions, the reaction system undergoes several main stages which are separately the incoming of nuclei, beginning of collisions, strongly-coupled quark-gluon plasma (sQGP) phase or hot-dense matter phase, mixed phase, and hadron gas. In the stage of the incoming of nuclei, two nuclei move toward each other in vacuum tunnel at nearly the speed of light and change the shape to pancake with the Lorentz contraction. The sQGP phase is extremely hot-dense matter and the system can be regarded as a fireball. Considering the effect of pressure gradient, the system begins to inflate and cool down. Then, the hadron matter appears until the system is hadronic. To understand the mechanism of nuclear reaction and the property of system evolution, it is necessary to investigate the characteristics of each

stage of collision process. The excitation and equilibrium degrees of the system are among very important characteristics [1–10].

To describe the excitation degree of the system, various temperatures of the system and the average transverse momentum ($\langle p_T \rangle$) of particles are used [11–18]. The various temperatures include, but are not limited to, i) the initial-state temperature (T_i) which reflects the temperature in the beginning of collisions of two nuclei, ii) the chemical freeze-out temperature (T_{ch}) which reflects the temperature at chemical freeze-out when inelastic collisions disappear, iii) the kinetic freeze-out or final-state temperature (T_{kin} or T_0) which reflects the temperature at kinetic freeze-out when elastic collisions disappear, and iv) the effective temperature (T_{eff}) which is not a “real” temperature, in which the influence of flow effect is not excluded compared with T_{kin} or T_0 . Different kinds of temperatures can be “measured” by different “thermometers” (methods).

As the earliest temperature in collisions, T_i is used to explore the secret of high-energy collisions [11–15]. As we know, T_i is the temperature of emission source or interacting system when the system undergoes the initial-

*qiwang-sxu@qq.com; 18303476022@163.com

†Correspondence: fuhuliu@163.com; fuhuliu@sxu.edu.cn

‡Correspondence: khkolimov@gmail.com; kh.olimov@uzsci.net

stage of collisions [19]. It is interesting for us to describe the excitation degree of the system by using T_i . Generally, from the transverse momentum (p_T) spectra or fitting the p_T spectra with different distributions or functions, we may obtain T_i . The Erlang distribution [20–22], Tsallis distribution [23, 24], Hagedorn function [25] are usually used, but in this paper, we only choose the Erlang distribution due to its origin of multiple sources in the multi-source thermal model [20–22]. In the special case, such as absent p_T spectra, the squared momentum transfer spectra are alternatively used. Obviously, T_i can not be obtained from the squared momentum transfer spectra directly unless the p_T spectra are transformed to them. From the fit to p_T spectra, $\langle p_T \rangle$ can be naturally abstracted.

In the transformation of p_T spectra to squared momentum transfer spectra [26], the Monte Carlo method is used. First of all, concrete p_T , satisfying the Erlang distribution [20–22], are produced. Then, the squared momentum transfers are calculated according to the relation between squared momentum transfers and p_T by using the Monte Carlo method. At last, the distribution of squared momentum transfer spectra are obtained and used to fit the experimental data for extracting $\langle p_T \rangle$ and T_i .

To describe the equilibrium degree of the system, one can use the Tsallis distribution [23, 24] or Hagedorn function [25] to fit p_T spectra directly. In the fitting process, the entropy index q can be extracted. The closer to 1 the entropy index q is, the higher the degree of equilibrium of the source or system is. The relation between the two distributions is that the former one covers the later one in which the mass is neglected. Because the universality, similarity, or common characteristics exist in high-energy collisions [27–36], some distributions used in large collision system can be also used in small collision system. Although the equilibrium degree is also important, it is not discussed in this work due to other topics being concerned. We think that the equilibrium degree is enough to use the concept of temperature.

Meson consists of a quark and anti-quark ($q\bar{q}$) and belongs to hadron. It takes part in the strong interaction and play an important role. Light meson refers to a kind of meson with low mass. The transverse momentum of light meson changes more sensitively than that of the heavy one. Therefore, the study of transverse momentum spectra of light mesons is very important to explore the reaction mechanism and evolution process of high-energy collisions.

Compared with large systems of high-energy nucleus-

nucleus collisions, small systems such as high-energy electron-proton, proton-proton, proton-nucleus collisions also produce abundant results. In particular, in electron-proton collisions, the scattered electron exchanges virtual photon (γ^*) with the target proton. Then, one may study high-energy γ^* induced proton collisions, that is γ^*p collisions, experimentally, theoretically as well as phenomenologically.

In this paper, the squared momentum transfer spectra of light mesons, π^0 , π^+ , η , and ρ^0 , produced in high-energy γ^*p collisions measured by the CLAS Collaboration [37–40] are fitted by the results originating from the Erlang p_T distribution with the Monte Carlo method. The CLAS experimental data are measured at different squared photon virtuality Q^2 and Bjorken variable x_B , where Q^2 and x_B will be discussed later in the subsection 2.3.

II. FORMALISM AND METHOD

i) *The Erlang distribution*

The Erlang distribution is a direct result of the multi-source thermal model [20–22]. One or two-component Erlang distribution can describe the narrow or wide p_T spectra of particles, where the narrow (wide) p_T spectra refers to range less than a few GeV/ c (more than 10 GeV/ c) [22]. The multi-source thermal model assumes that multiple sources are formed in high-energy collisions. These sources can be nucleons or partons if we study the formation of nucleon clusters (nuclear fragments) or particles.

In this work, we assume that a few (n_s) partons (partons-like) contribute to p_T of a given particle [22]. The contribution of the j -th parton is assumed to be an exponential function with variable p_{tj} which depends on j , and average value $\langle p_t \rangle$ which is independent of j . We have the normalized exponential function

$$f(p_{tj}) = \frac{1}{\langle p_t \rangle} \exp\left(-\frac{p_{tj}}{\langle p_t \rangle}\right). \quad (1)$$

Here, $\langle p_t \rangle$ represents the average contribution of participant partons to $\langle p_T \rangle$ of the considered particles.

The contribution sum ($p_{t1} + p_{t2} + \dots + p_{tn_s}$) of n_s partons is p_T of a given particle. The result convoluting the contributions of n_s partons is the Erlang distribution. We have the Erlang p_T distribution to be

$$f(p_T) = \frac{1}{N} \frac{dN}{dp_T} = \frac{p_T^{n_s-1}}{(n_s-1)!\langle p_t \rangle^{n_s}} \exp\left(-\frac{p_T}{\langle p_t \rangle}\right). \quad (2)$$

Here N is the number of particles, and the form of $(1/N)dN/dp_T$ results in the normalization of $f(p_T)$ to 1. In fact, the normalization of the Erlang distribution is naturally 1.

We would like to emphasize here the difference between “ n_s ”, the number of partons and “ N ”, the number of particles. In γ^*p collisions, if three quarks in the proton contributed to p_T , we have $n_s = 3$. If another $q\bar{q}$ pair also contributed to p_T , we have $n_s = 3 + 2 = 5$. Even in nucleus-nucleus collisions, the value of n_s is not large due to it being determined by the number of contributor partons in a nucleon-nucleon pair, but not collision system itself. This makes sense, in the Fock’s first two terms of the development of the wave function of the proton, as composed by 3 quarks and then 3 quarks plus a $q\bar{q}$ pair [41, 42]. As for N , its value may be small in small collision system or peripheral nucleus-nucleus collisions. The value of N may be very large in central nucleus-nucleus collisions at high energy.

ii) *Average transverse momentum and initial-state temperature*

As we know, both the average transverse momentum $\langle p_T \rangle$ and initial-state temperature T_i [11–15] describe the excitation degree of the system. In particular, in the Erlang distribution, $\langle p_T \rangle$ can be easily obtained by

$$\langle p_T \rangle = \int_0^\infty p_T f(p_T) dp_T = n_s \langle p_t \rangle, \quad (3)$$

where $f(p_T)$ is normalized to 1. Similarly, $\langle p_t \rangle$ reflects the excitation degree of participant partons.

According to refs. [43–45], with a color string percolation method [46], T_i can be regarded as

$$T_i = \sqrt{\frac{\langle p_T^2 \rangle}{2F(\xi)}}, \quad (4)$$

where

$$\langle p_T^2 \rangle = \int_0^\infty p_T^2 f(p_T) dp_T \quad (5)$$

due to $f(p_T)$ is normalized to 1 and $\sqrt{\langle p_T^2 \rangle}$ is the root-mean-square of p_T . In Eq. (4), $F(\xi)$ is the color suppression factor [46].

In the process of using color string method to obtain T_i in this work, only one string is used, i.e. $F(\xi) = 1$, in the formation of particle. Although there are probability to have any other strings, they do not affect noticeably T_i . If we consider other strings, according to ref. [46], one has the minimum $F(\xi) \approx 0.6$. This will cause the maximum increase of 29.1% in T_i . Considering the

fraction of one string is very large, that of two strings is relative small, and that of multiple strings is very small, the increase in T_i will be much smaller than 29.1%.

iii) *The squared momentum transfer*

In the center-of-mass reference frame, in two-body process $2 + 1 \rightarrow 4 + 3$ or two-body-like process of high-energy collisions, there are three Mandelstam variables defined based on the four-momenta of these particles. They have the forms to be

$$s = -(P_1 + P_2)^2 = -(P_3 + P_4)^2, \quad (6)$$

$$t = -(P_1 - P_3)^2 = -(-P_2 + P_4)^2, \quad (7)$$

$$u = -(P_1 - P_4)^2 = -(-P_2 + P_3)^2, \quad (8)$$

where P_1 , P_2 , P_3 , and P_4 are four-momenta of particles 1 (target proton), 2 (incident γ^*), 3 (emitted nucleon), and 4 (emitted meson), respectively. Here, we assume that particle 1 is incident along the Oz direction and particle 2 is incident along the opposite direction. After collisions, particle 3 is emitted with angle θ relative to the Oz direction and particle 4 is emitted along the opposite direction.

The three Mandelstam variables have different physical meaning. For instance, \sqrt{s} refers to the center-of-mass energy, and $-u$ is defined as the squared momentum transfer between particles 1 and 4. Here, selected variable $-t$ (the squared momentum transfer between particles 1 and 3) is calculated to fit the experimental data. For convenience, we have

$$\begin{aligned} |t| &= |(E_1 - E_3)^2 - (\vec{p}_1 - \vec{p}_3)^2| \\ &= \left| m_1^2 + m_3^2 - 2E_1 \sqrt{\left(\frac{p_{3T}}{\sin \theta}\right)^2 + m_3^2} \right. \\ &\quad \left. + 2\sqrt{E_1^2 - m_1^2} \frac{p_{3T}}{\tan \theta} \right|, \end{aligned} \quad (9)$$

where E_1 and E_3 , \vec{p}_1 and \vec{p}_3 , as well as m_1 and m_3 are the energy, momentum, and rest mass of particles 1 and 3, respectively. In addition, p_{3T} referred to be perpendicular to the Oz direction component of the transverse momentum of particle 3, which obeys the Erlang distribution, that is Eq. (2) in which $p_T = p_{3T}$.

In this paper, the squared momentum transfer spectra of light meson at different squared photon virtuality Q^2 and Bjorken variable x_B are fitted by calculated results with the Monte Carlo method. Here, Q^2 is a reflection of hard scale of reaction [47–54]. The harder the reaction

is, the higher the excitation degree is. In fact, Q^2 is the absolute value of the squared mass of γ^* (particle 2) that is exchanged between the scattered electron and the target proton (particle 1), and it effectively represents the transverse size of the probe [38]. In addition, $-Q^2$ is also the squared momentum transfer to the target proton (particle 1) by the scattered electron [37].

As for the Bjorken variable x_B , it represents contrarily the momentum of particle 1. The lower the x_B is, the higher the momentum of particle 1 is. Generally, $x_B = Q^2/(2P_2 \cdot \sqrt{-Q^2}) \propto Q$ [37]. In a symmetric frame, importing ξ' as skewness, it is half of the longitudinal momentum fraction transferred to the struck parton. The skewness ξ' can be used to express x_B approximately. That is $x_B \approx 2\xi'/(1+\xi')$ [37].

iv) The process of Monte Carlo calculations

In the calculations of squared momentum transfer, the analytical expression of p_T distribution is difficult to be transformed to that of squared momentum transfer distribution directly by using Eq. (9). Alternatively, we may use the Monte Carlo method to transform p_T to squared momentum transfer. Let $R_{1,2}$ and $r_{1,2,3,\dots,n_s}$ be random numbers distributed evenly in $[0,1]$. Then, many concrete transverse momentum p_{3T} satisfied with Eq. (2) and θ are produced. Other quantities such as E_1 , m_1 , and m_3 in the equation are fixed, though E_1 is treated as a parameter in the present work.

Generally, we may solve the equation

$$\int_0^{p_T} f(p'_T) dp'_T < R_1 < \int_0^{p_T+\delta p_T} f(p'_T) dp'_T, \quad (10)$$

where δp_T is a small shift relative to p_T . Conveniently, there is a simpler expression due to Eqs. (1) and (2). In fact, solving the equation

$$\int_0^{p_{tj}} f(p'_{tj}) dp'_{tj} = r_j \quad (j = 1, 2, 3, \dots, n_s), \quad (11)$$

we have

$$p_{tj} = -\langle p_t \rangle \ln r_j \quad (j = 1, 2, 3, \dots, n_s). \quad (12)$$

The simpler expression is

$$p_T = \sum_{j=1}^{n_s} p_{tj} = -\langle p_t \rangle \sum_{j=1}^{n_s} \ln r_j = -\langle p_t \rangle \ln \left(\prod_{j=1}^{n_s} r_j \right). \quad (13)$$

The distribution of θ satisfies with the half-sine function

$$f_\theta(\theta) = \frac{1}{2} \sin \theta \quad (14)$$

which is obtained under the assumption of isotropic emission in the source's rest frame. Solving the equation

$$\int_0^\theta f_\theta(\theta') d\theta' = R_2, \quad (15)$$

we have

$$\theta = 2 \arcsin \left(\sqrt{R_2} \right) \quad (16)$$

which is needed in the calculations.

We have checked the consistency and correctness of the above expressions in the Monte Carlo method in terms of illustration which is not presented here. After obtaining concrete values of p_{3T} and θ , and using E_1 , m_1 , and m_3 , the value of $|t|$ can be obtained from Eq. (9). Through repeating the calculations many times, the distribution of $|t|$ is obtained statistically. Based on the method of least squares, the parameter $\langle p_t \rangle$ and n_s are extracted naturally. Meanwhile, T_i can be obtained from Eq. (4) and $\langle p_T \rangle$ ($\langle p_T^2 \rangle$) can be obtained from Eq. (3) [(5)] or from the statistics. The errors of parameters are obtained by the general method of statistical analysis.

It should be noted that the above Monte Carlo calculation is only performed in the transformation from transverse momentum to $|t|$, in which the physics process such as the radiative corrections for reactions induced by electrons has been taken into account naturally. In fact, the effects of the mentioned process and all other processes are included in the Erlang distribution which is a result of multi-factor interactions. In other words, the Monte Carlo calculation used here is not a simulation for the system evolution from initial to final stages, but the numerical transformation in the final stage.

III. RESULTS AND DISCUSSION

A. Comparison with data

Figure 1 shows the differential cross-section, $d\sigma/d|t|$, in squared momentum transfer $|t|$ of $\gamma^*p \rightarrow \pi^0p$ process produced in 5.75 GeV electron beam induced collisions in a 2.5 cm long liquid-hydrogen target (ep collisions at beam energy of 5.75 GeV) in different ranges of squared photon virtuality, $1.0 < Q^2 < 1.5$, $1.5 < Q^2 < 2.0$, $2.0 < Q^2 < 2.5$, $2.5 < Q^2 < 3.0$, $3.0 < Q^2 < 3.5$, $3.5 < Q^2 < 4.0$, and $4.0 < Q^2 < 4.6 \text{ GeV}^2$, from bottom to up sub-panels, as well as in different ranges of Bjorken variable, $0.10 < x_B < 0.15$, $0.15 < x_B < 0.20$, $0.20 < x_B < 0.25$, $0.25 < x_B < 0.30$, $0.30 < x_B < 0.38$, $0.38 < x_B < 0.48$, and $0.48 < x_B < 0.58$, from left to

right sub-panels. The sample at the top-left sub-panel shows repeatedly the result in the range of squared photon virtuality, $1.5 < Q^2 < 2.0 \text{ GeV}^2$, and the range of Bjorken variable, $0.20 < x_B < 0.25$, as an example. The symbols represent the experimental data measured by the CLAS Collaboration [37] and the curves are the statistical results of squared momentum transfer $|t|$.

In Eq. (9), p_{3T} satisfies the Erlang distribution [Eq. (2)] and we obtain it by the Monte Carlo method [Eq. (13)]. Then, the squared momentum transfer $|t|$ is obtained statistically. In the fitting process, two main parameters, i.e. the average transverse momentum $\langle p_t \rangle$ contributed by each participant parton and the number n_s of participant partons are extracted naturally. To obtain a better fit result, E_1 is extracted as an insensitive parameter. In addition, a non-free parameter is the normalization constant σ_0 . The values of parameters with selection condition (Q^2 and x_B), χ^2 , and the number of degree of freedom (ndof) are listed in Table 1, where the number of parameters is always 4 which includes E_1 , $\langle p_t \rangle$, n_s , and σ_0 . In the case of ndof being less than or equal to the number of parameters, we obtain the curve from a ‘‘prediction’’ or extrapolation based on other reasonable fits in which the tendency of parameters is available. Meanwhile, in these cases, the number of points (nop) is given in a bracket to replace ndof in the table. One can see that the values of χ^2 are small in most cases, though the (necessary) dense log scale is not easy to judge. The model results are in agreement with the experimental data. From the values of parameters, the average transverse momentum $\langle p_T \rangle$ and initial temperature T_i are obtained naturally.

Figure 2 presents the differential cross-section, $d\sigma/d|t|$, in $|t|$ of $\gamma^*p \rightarrow \pi^+n$ process produced in ep collisions at beam energy of 6 GeV at different squared photon virtuality, $Q^2 = 1.75, 2.05, 2.35, 2.65, 2.95, 3.35, 3.85, \text{ and } 4.35 \text{ GeV}^2$, as well as at different Bjorken variable, $x_B = 0.25, 0.31, 0.37, 0.43, 0.49, \text{ and } 0.55$. The symbols represent the experimental data measured by the CLAS Collaboration [38]. As those in Figure 1, the curves in Figure 2 are also the statistical results of $|t|$ in which p_{3T} satisfies the Erlang distribution and is obtained by the Monte Carlo method. The values of parameters with selection condition (Q^2 and x_B), χ^2 , and nop are listed in Table 1. One can see that the model results are in agreement with the experimental data.

Figure 3 displays the differential cross-section, $d\sigma/d|t|$, in $|t|$ of $\gamma^*p \rightarrow \eta p$ process produced in ep collisions at beam energy of 5.75 GeV in different Q^2 and x_B ranges shown in the panel. As an example, the sample

at the top-left sub-panel shows repeatedly the result in $1.5 < Q^2 < 2.0 \text{ GeV}^2$ and $0.20 < x_B < 0.25$. The symbols represent the experimental data measured by the CLAS Collaboration [39]. The curves are the statistical results of $|t|$ in which p_{3T} satisfies the Erlang distribution and is obtained by the Monte Carlo method. The values of parameters with selection condition (Q^2 and x_B), χ^2 , and nop are listed in Table 2. One can see that the model results are in agreement with the experimental data.

Similar to Figures 1–3, Figure 4 presents the differential cross-section, $d\sigma/d|t|$, in $|t|$ of $\gamma^*p \rightarrow \rho^0 p$ process produced in ep collisions at beam energy of 5.754 GeV in different Q^2 and x_B ranges shown in the panel. As an example, the sample at the top-left sub-panel shows repeatedly the result in $2.8 < Q^2 < 3.1 \text{ GeV}^2$ and $0.40 < x_B < 0.46$ range. The symbols represent the experimental data measured by the CLAS Collaboration [40]. The curves are the statistical results of $|t|$ in which p_{3T} satisfies the Erlang distribution and is obtained by the Monte Carlo method. The values of parameters with selection condition (Q^2 and x_B), χ^2 , and nop are listed in Table 2. One can see that the model results are in agreement with the experimental data.

B. Parameter tendency and discussion

In Figures 1–4, the cross-sections for $\pi^0 p$, $\pi^+ n$, ηp , and $\rho^0 p$ are fitted to show some differences in concrete values and parameters, and some common features among them in the tendency of curves also appear. This is caused by the fact that different channels have different fraction ratios, and all of them are from the same ep collisions, though the collision energies are slightly different.

The dependences of $\langle p_T \rangle$ (a, c, e, g) and T_i (b, d, f, h) on Q^2 in γ^*p collisions with different emitted channels [$\pi^0 p$ (a, b), $\pi^+ n$ (c, d), ηp (e, f), and $\rho^0 p$ (g, h)] are shown in Figure 5, where $\langle p_T \rangle = n_s \langle p_t \rangle$ due to Tables 1 and 2 and the values of T_i are from Tables 1 and 2. Different symbols represent the results for different x_B . One can see that $\langle p_T \rangle$ and T_i increase generally with an increase in Q^2 . Because Q^2 represents the hard scale (violent degree) of collisions and a harder scale results in a higher excitation degree, it is natural that larger $\langle p_T \rangle$ and T_i appear at higher Q^2 .

Figure 6 is similar to Figure 5, but it shows the dependences of $\langle p_T \rangle$ (a, c, e, g) and T_i (b, d, f, h) on x_B in γ^*p collisions with emitted channels $\pi^0 p$ (a, b), $\pi^+ n$ (c, d), ηp (e, f), and $\rho^0 p$ (g, h). Different symbols represent

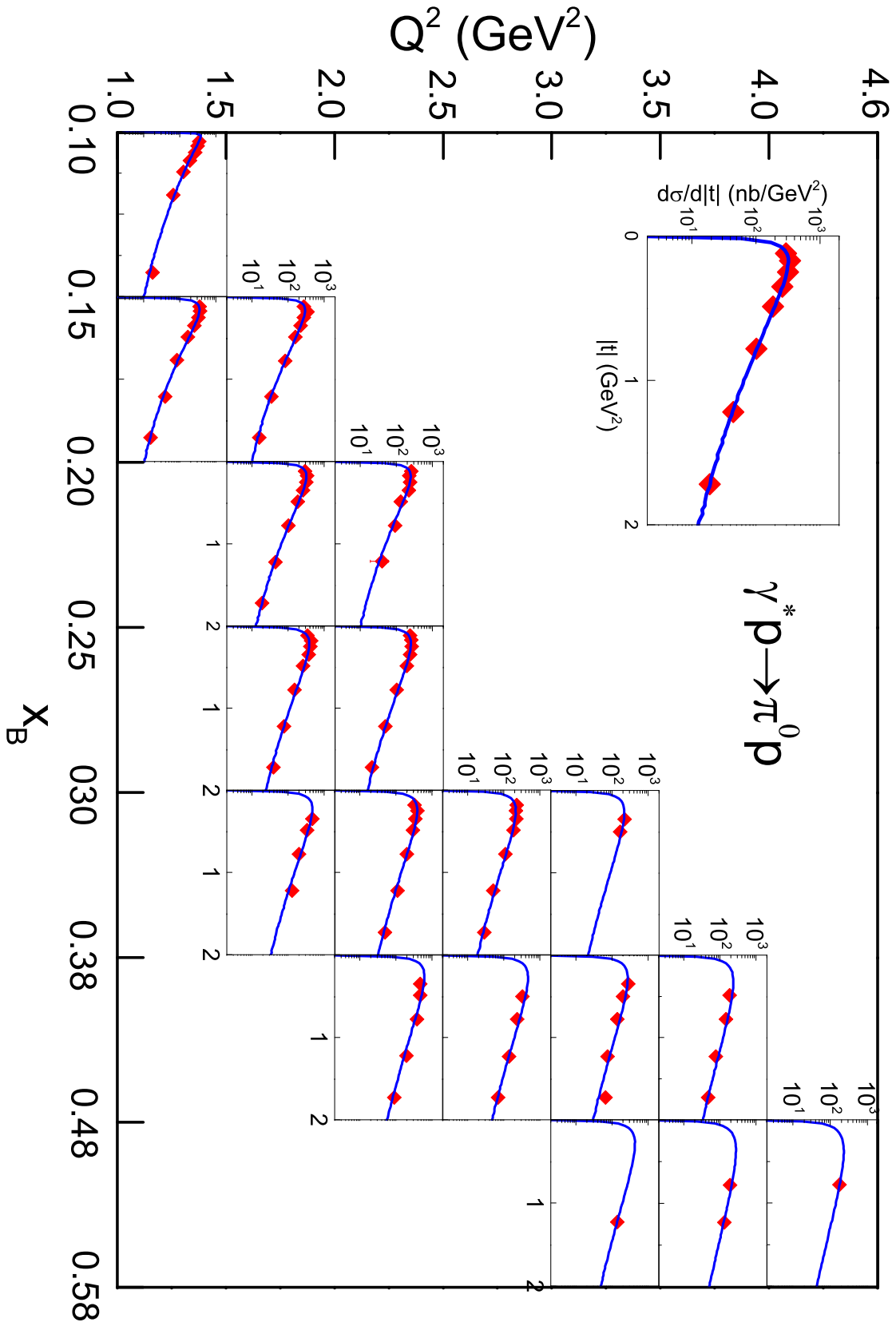


Fig. 1. The differential cross-section $d\sigma/d|t|$ in $|t|$ of $\gamma^*p \rightarrow \pi^0p$ process produced in ep collisions at beam energy of 5.75 GeV in different ranges of Q^2 and x_B shown in the panels. The sample at the top-left sub-panel shows repeatedly the result in $1.5 < Q^2 < 2.0$ GeV² and $0.20 < x_B < 0.25$ as an example. The symbols represent the experimental data measured by the CLAS Collaboration [37] and the curves are the statistical results of $|t|$ [Eq. (9)] in which p_{3T} satisfies the Erlang distribution [Eq. (2)] and can be obtained with the Monte Carlo method [Eq. (13)].

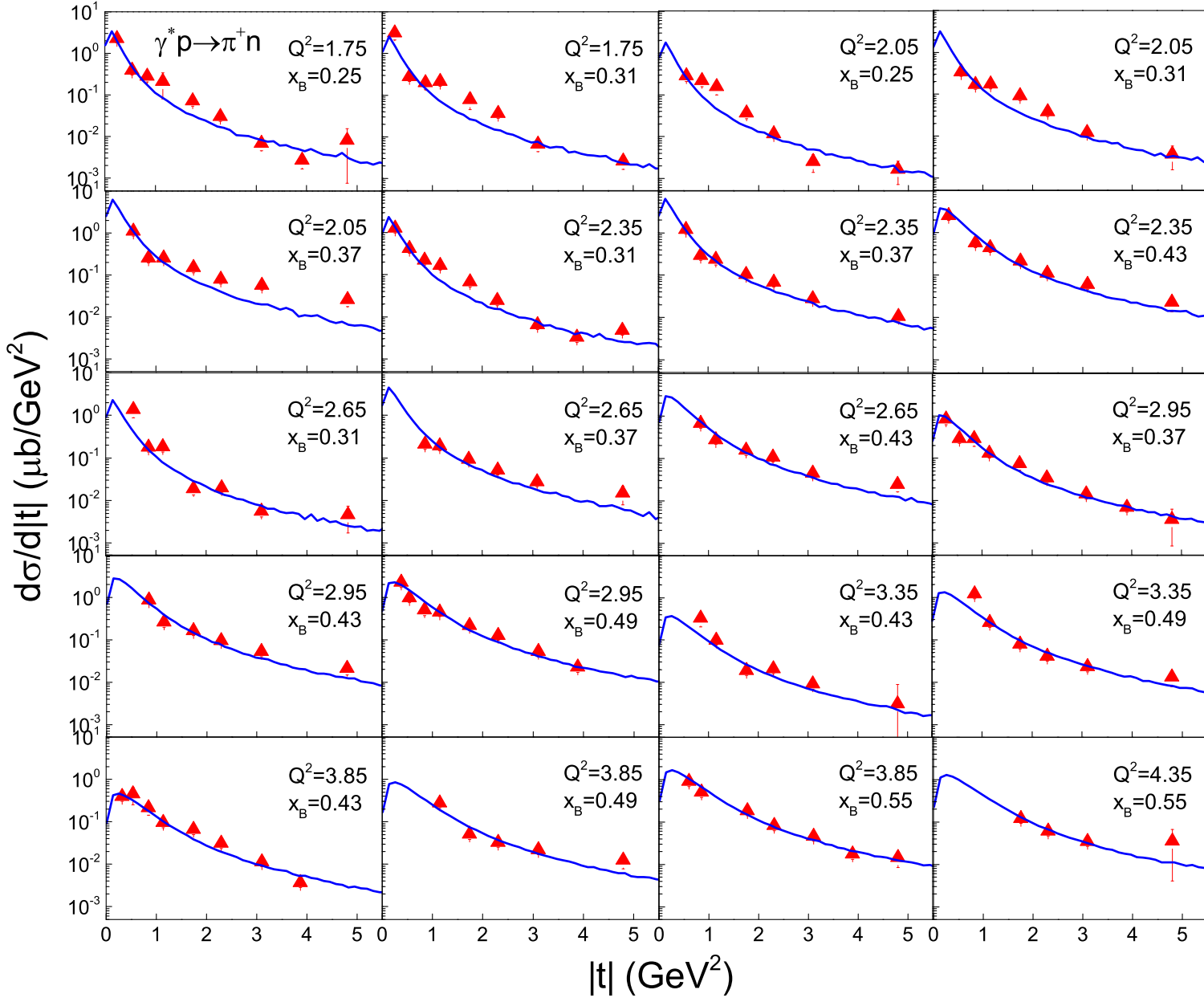


Fig. 2. The differential cross-section $d\sigma/d|t|$ in $|t|$ of $\gamma^* p \rightarrow \pi^+ n$ process produced in ep collisions at beam energy of 6 GeV at different Q^2 and x_B shown in the panels. The symbols represent the experimental data measured by the CLAS Collaboration [38] and the curves are the statistical results obtained as those in Figure 1.

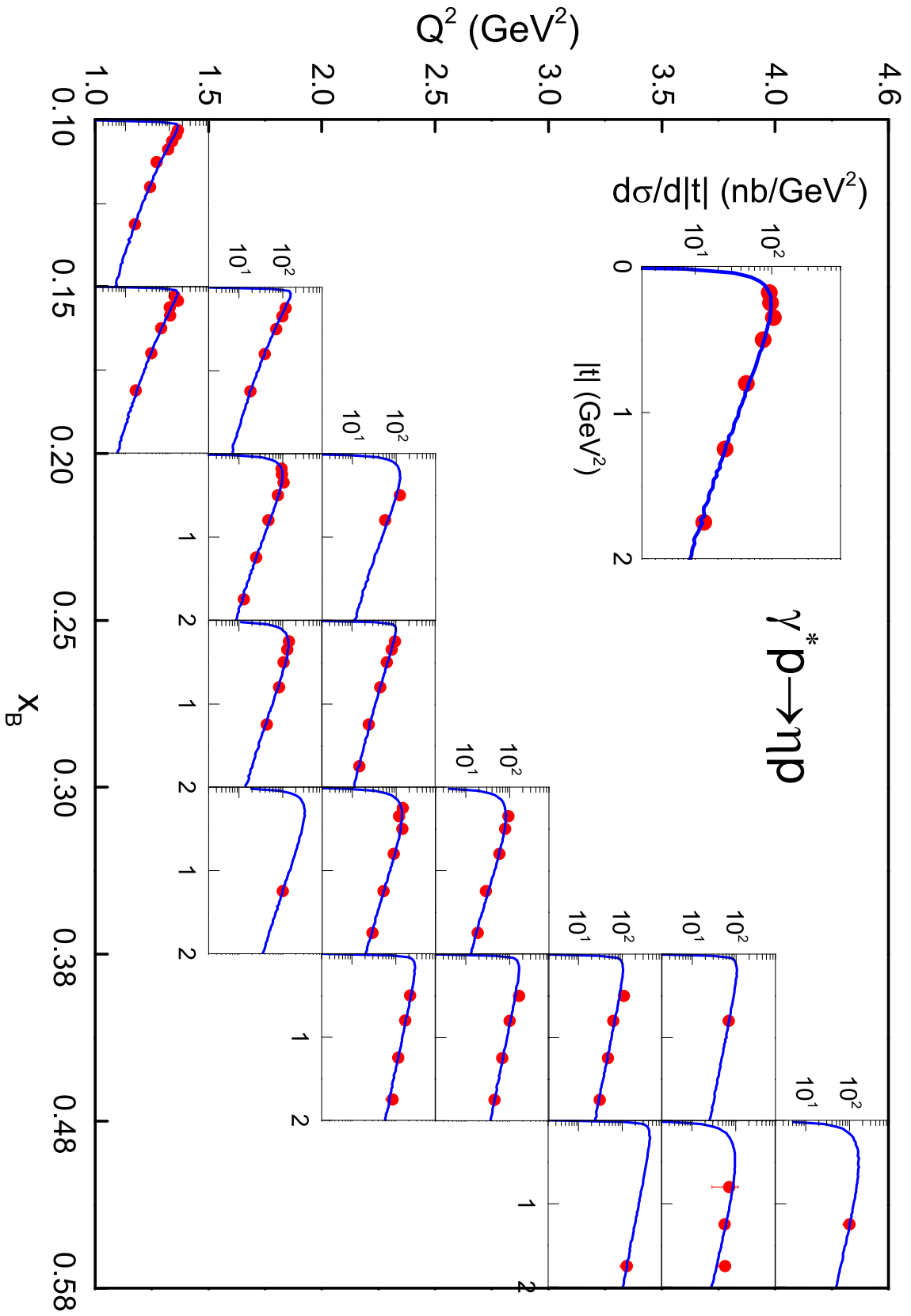


Fig. 3. The differential cross-section $d\sigma/d|t|$ in $|t|$ of $\gamma^*p \rightarrow \eta p$ process produced in ep collisions at beam energy of 5.75 GeV in different Q^2 and x_B ranges shown in the panels. As an example, the sample at the top-left sub-panel shows repeatedly the result in $1.5 < Q^2 < 2.0$ GeV² and $0.20 < x_B < 0.25$. The symbols represent the experimental data measured by the CLAS Collaboration [39] and the curves are the statistical results obtained as those in Figure 1.

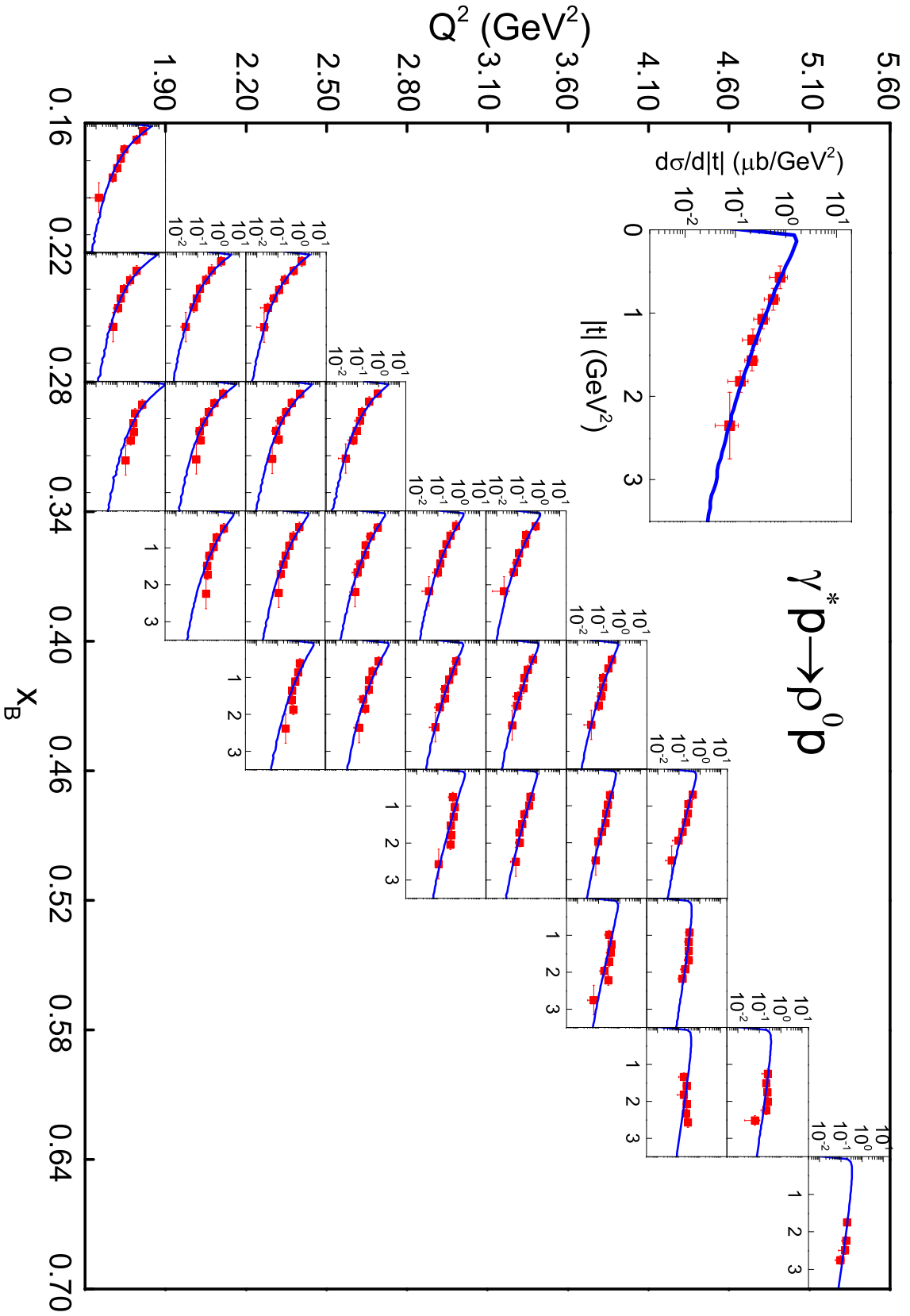


Fig. 4. The differential cross-section $d\sigma/d|t|$ in $|t|$ of $\gamma^* p \rightarrow \rho^0 p$ process produced in ep collisions at beam energy of 5.754 GeV in different Q^2 and x_B ranges shown in the panels. As an example, the sample at the top-left sub-panel shows repeatedly the result in $2.8 < Q^2 < 3.1 \text{ GeV}^2$ and $0.40 < x_B < 0.46$. The symbols represent the experimental data measured by the CLAS Collaboration [40] and the curves are the statistical results obtained as those in Figure 1.

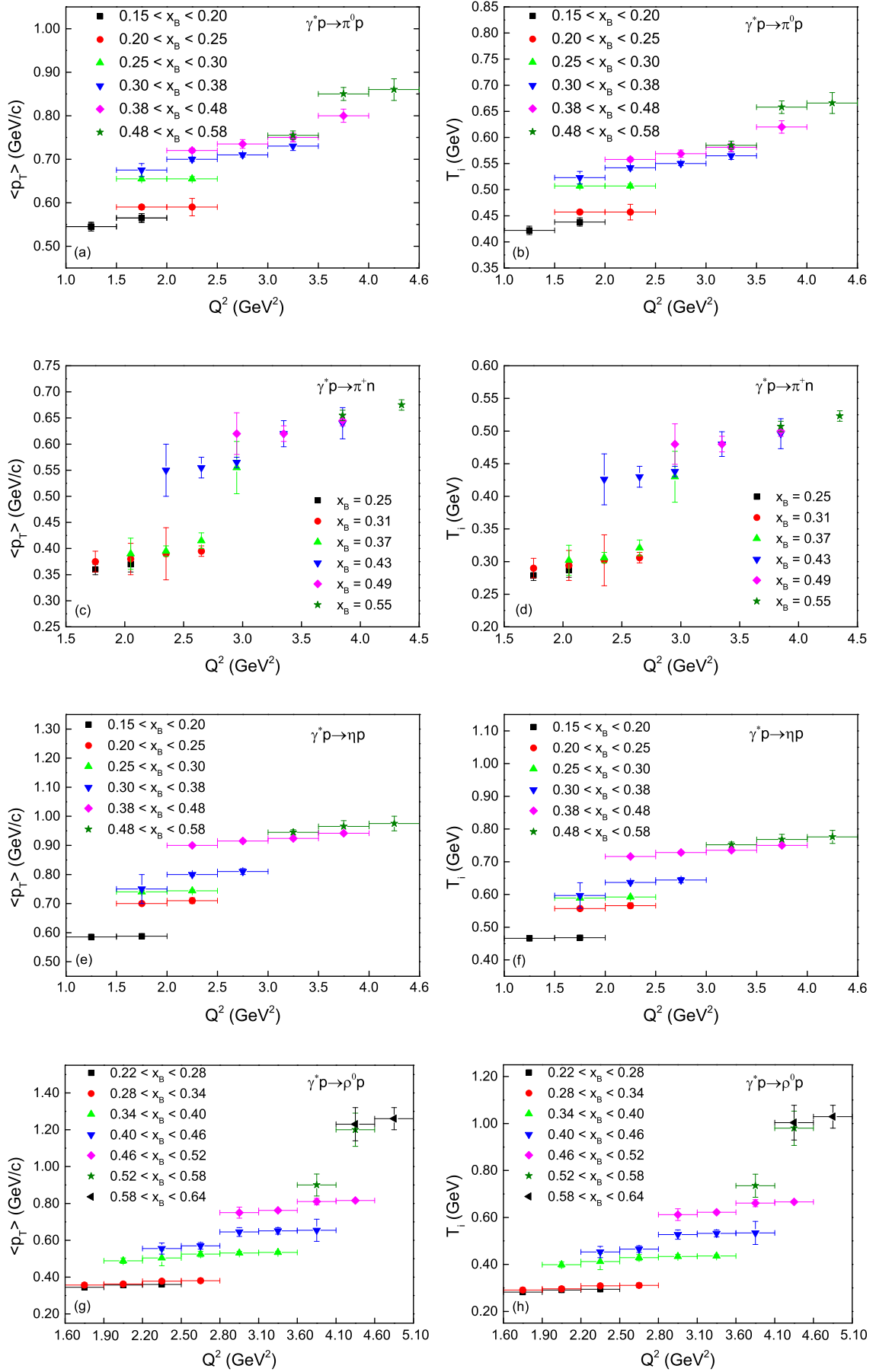


Fig. 5. The dependences of $\langle p_T \rangle$ (a, c, e, g) and T_i (b, d, f, h) on Q^2 in γ^*p collisions with emitted channels $\pi^0 p$ (a, b), $\pi^+ n$ (c, d), ηp (e, f), and $\rho^0 p$ (g, h). Different symbols represent the results for different x_B .

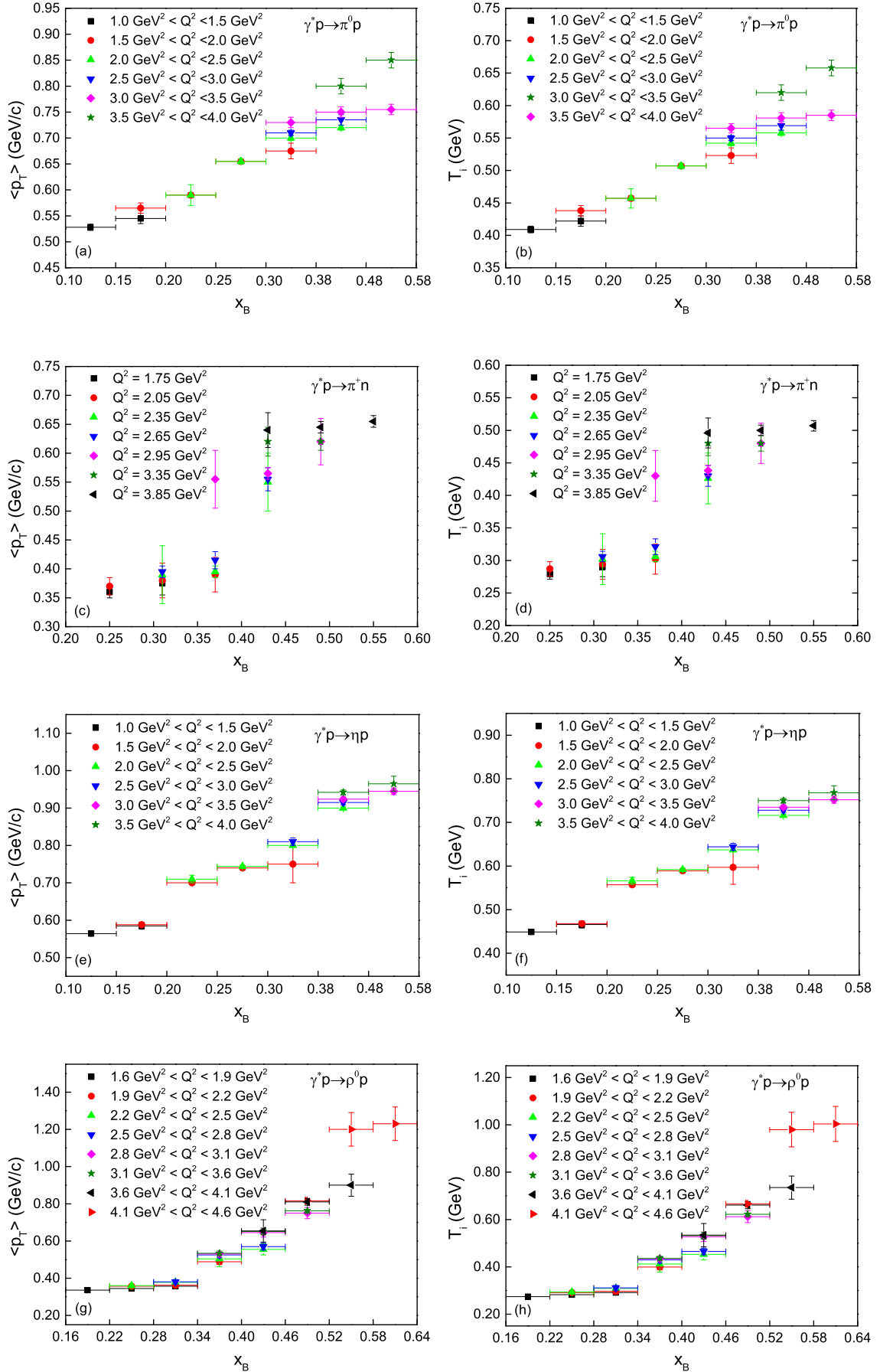


Fig. 6. The dependences of $\langle p_T \rangle$ (a, c, e, g) and T_i (b, d, f, h) on x_B in $\gamma^* p$ collisions with emitted channels $\pi^0 p$ (a, b), $\pi^+ n$ (c, d), ηp (e, f), and $\rho^0 p$ (g, h). Different symbols represent the results for different Q^2 .

Table 1. Values of E_1 , $\langle p_t \rangle$, n_s , σ_0 , T_i , and χ^2/ndof corresponding to the curves in Figures 1 and 2, where n_s is constrained to be integer with uncertainty of 0 which is not listed in the table. The number of parameters is always 4 which includes E_1 , $\langle p_t \rangle$, n_s , and σ_0 . In the case of ndof being less than or equal to the number of parameters, we obtain the curve from a ‘‘prediction’’ or extrapolation based on other reasonable fits, and show the corresponding nop in a bracket to replace ndof. The value of χ^2 is rounded to an integer, or one significant digit if the integer is 0.

Collisions	Q^2 (GeV)	x_B	E_1 (GeV)	$\langle p_t \rangle$ (GeV/c)	n_s	σ_0 (μb)	T_i (GeV)	$\chi^2/\text{ndof}(\text{nop})$
$\gamma^*p \rightarrow \pi^0 p$	(1.0, 1.5)	(0.10, 0.15)	$0.945_{-0.007}^{+0.015}$	0.176 ± 0.002	3	0.195 ± 0.005	0.409 ± 0.005	7/11
	(1.0, 1.5)	(0.15, 0.20)	0.945 ± 0.004	0.109 ± 0.002	5	0.220 ± 0.008	0.422 ± 0.008	11/12
	(1.5, 2.0)	(0.15, 0.20)	0.945 ± 0.005	0.113 ± 0.002	5	0.197 ± 0.003	0.438 ± 0.008	5/12
	(1.5, 2.0)	(0.20, 0.25)	0.945 ± 0.003	0.118 ± 0.001	5	0.232 ± 0.010	0.457 ± 0.004	6/12
	(2.0, 2.5)	(0.20, 0.25)	$0.945_{-0.007}^{+0.015}$	0.118 ± 0.004	5	0.175 ± 0.005	0.457 ± 0.015	7/11
	(1.5, 2.0)	(0.25, 0.30)	0.945 ± 0.001	0.131 ± 0.001	5	0.335 ± 0.013	0.507 ± 0.004	12/12
	(2.0, 2.5)	(0.25, 0.30)	0.945 ± 0.001	0.131 ± 0.001	5	0.220 ± 0.007	0.507 ± 0.004	6/12
	(1.5, 2.0)	(0.30, 0.38)	0.945 ± 0.002	0.135 ± 0.003	5	0.430 ± 0.020	0.523 ± 0.012	7/(4)
	(2.0, 2.5)	(0.30, 0.38)	0.945 ± 0.003	0.140 ± 0.001	5	0.380 ± 0.013	0.542 ± 0.004	10/11
	(2.5, 3.0)	(0.30, 0.38)	0.945 ± 0.002	0.142 ± 0.001	5	0.215 ± 0.010	0.550 ± 0.004	6/11
	(3.0, 3.5)	(0.30, 0.38)	0.945 ± 0.003	0.146 ± 0.002	5	0.230 ± 0.011	0.565 ± 0.007	0.8/(2)
	(2.0, 2.5)	(0.38, 0.48)	0.945 ± 0.005	0.144 ± 0.001	5	0.630 ± 0.030	0.558 ± 0.004	14/9
	(2.5, 3.0)	(0.38, 0.48)	0.945 ± 0.002	0.147 ± 0.002	5	0.500 ± 0.022	0.569 ± 0.007	17/(4)
	(3.0, 3.5)	(0.38, 0.48)	0.945 ± 0.001	0.150 ± 0.002	5	0.300 ± 0.016	0.581 ± 0.008	29/9
	(3.5, 4.0)	(0.38, 0.48)	0.945 ± 0.005	0.160 ± 0.003	5	0.290 ± 0.012	0.620 ± 0.012	2/(4)
	(3.0, 3.5)	(0.48, 0.58)	0.945 ± 0.001	0.151 ± 0.002	5	0.480 ± 0.023	0.585 ± 0.008	0.1/(1)
	(3.5, 4.0)	(0.48, 0.58)	0.945 ± 0.002	0.170 ± 0.003	5	0.380 ± 0.014	0.658 ± 0.012	1/(2)
(4.0, 4.6)	(0.48, 0.58)	0.945 ± 0.003	0.172 ± 0.005	5	0.320 ± 0.015	0.666 ± 0.020	0.01/(1)	
$\gamma^*p \rightarrow \pi^+ n$	1.75	0.25	0.950 ± 0.005	0.072 ± 0.002	5	1.200 ± 0.050	0.279 ± 0.008	18/13
	1.75	0.31	0.950 ± 0.010	0.075 ± 0.004	5	0.950 ± 0.030	0.290 ± 0.015	28/12
	2.05	0.25	0.950 ± 0.010	0.074 ± 0.003	5	0.650 ± 0.020	0.287 ± 0.011	16/11
	2.05	0.31	0.950 ± 0.003	0.076 ± 0.006	5	1.200 ± 0.040	0.294 ± 0.023	29/11
	2.05	0.37	0.950 ± 0.010	0.078 ± 0.006	5	2.400 ± 0.090	0.302 ± 0.023	27/11
	2.35	0.31	0.950 ± 0.004	0.078 ± 0.010	5	0.900 ± 0.020	0.302 ± 0.039	24/12
	2.35	0.37	0.950 ± 0.010	0.079 ± 0.002	5	2.500 ± 0.080	0.306 ± 0.008	9/11
	2.35	0.43	0.950 ± 0.006	0.110 ± 0.010	5	2.500 ± 0.100	0.426 ± 0.039	10/11
	2.65	0.31	0.950 ± 0.010	0.079 ± 0.002	5	0.900 ± 0.030	0.306 ± 0.008	16/11
	2.65	0.37	0.950 ± 0.008	0.083 ± 0.003	5	1.900 ± 0.050	0.321 ± 0.012	14/10
	2.65	0.43	0.950 ± 0.010	0.111 ± 0.004	5	2.000 ± 0.070	0.430 ± 0.016	9/10
	2.95	0.37	0.950 ± 0.010	0.111 ± 0.010	5	0.700 ± 0.020	0.430 ± 0.039	22/13
	2.95	0.43	0.950 ± 0.004	0.113 ± 0.002	5	2.000 ± 0.090	0.438 ± 0.008	10/10
	2.95	0.49	0.950 ± 0.012	0.124 ± 0.008	5	1.900 ± 0.070	0.480 ± 0.031	15/12
	3.35	0.43	0.950 ± 0.010	0.124 ± 0.005	5	0.300 ± 0.020	0.480 ± 0.019	11/10
	3.35	0.49	0.950 ± 0.010	0.124 ± 0.003	5	1.100 ± 0.080	0.480 ± 0.012	9/10
	3.85	0.43	0.950 ± 0.006	0.128 ± 0.006	5	0.400 ± 0.030	0.496 ± 0.023	10/12
3.85	0.49	0.950 ± 0.003	0.129 ± 0.002	5	0.750 ± 0.040	0.500 ± 0.008	8/9	
3.85	0.55	0.950 ± 0.003	0.131 ± 0.002	5	1.500 ± 0.080	0.507 ± 0.008	4/11	
4.35	0.55	0.950 ± 0.002	0.135 ± 0.002	5	1.200 ± 0.060	0.523 ± 0.008	1/(4)	

the results for different Q^2 . One can see that $\langle p_T \rangle$ and T_i increase generally with an increase in x_B . Because $x_B \propto Q$, we may think that x_B also represents the hard

scale of collisions and a harder scale results in a higher excitation degree. It is understandable that larger $\langle p_T \rangle$ and T_i appear at higher x_B .

Table 2. Same as Table 1, but corresponding to the curves in Figures 3 and 4.

Collisions	Q^2 (GeV)	x_B	E_1 (GeV)	$\langle p_t \rangle$ (GeV/c)	n_s	σ_0 (μb)	T_i (GeV)	$\chi^2/\text{ndof}(\text{nop})$
$\gamma^*p \rightarrow \eta p$	(1.0, 1.5)	(0.10, 0.15)	0.955 ± 0.005	0.188 ± 0.001	3	0.093 ± 0.004	0.449 ± 0.003	7/11
	(1.0, 1.5)	(0.15, 0.20)	0.955 ± 0.003	0.195 ± 0.003	3	0.098 ± 0.005	0.466 ± 0.008	5/11
	(1.5, 2.0)	(0.15, 0.20)	0.955 ± 0.002	0.196 ± 0.001	3	0.098 ± 0.007	0.468 ± 0.003	1/9
	(1.5, 2.0)	(0.20, 0.25)	0.955 ± 0.001	0.140 ± 0.001	5	0.098 ± 0.003	0.557 ± 0.004	3/11
	(2.0, 2.5)	(0.20, 0.25)	0.955 ± 0.010	0.142 ± 0.002	5	0.125 ± 0.008	0.566 ± 0.008	2/(2)
	(1.5, 2.0)	(0.25, 0.30)	0.955 ± 0.002	0.148 ± 0.001	5	0.147 ± 0.008	0.589 ± 0.004	3/9
	(2.0, 2.5)	(0.25, 0.30)	0.955 ± 0.005	0.248 ± 0.001	3	0.100 ± 0.006	0.592 ± 0.003	1/11
	(1.5, 2.0)	(0.30, 0.38)	0.955 ± 0.010	0.150 ± 0.010	5	0.354 ± 0.015	0.597 ± 0.039	0.04/(1)
	(2.0, 2.5)	(0.30, 0.38)	0.955 ± 0.004	0.160 ± 0.001	5	0.170 ± 0.005	0.637 ± 0.004	4/10
	(2.5, 3.0)	(0.30, 0.38)	0.955 ± 0.003	0.162 ± 0.002	5	0.105 ± 0.006	0.644 ± 0.008	3/9
	(2.0, 2.5)	(0.38, 0.48)	0.955 ± 0.002	0.300 ± 0.001	3	0.390 ± 0.018	0.716 ± 0.003	0.3/(1)
	(2.5, 3.0)	(0.38, 0.48)	0.955 ± 0.002	0.305 ± 0.002	3	0.240 ± 0.013	0.728 ± 0.005	2/(4)
	(3.0, 3.5)	(0.38, 0.48)	0.955 ± 0.002	0.308 ± 0.002	3	0.155 ± 0.012	0.735 ± 0.005	2/(4)
	(3.5, 4.0)	(0.38, 0.48)	0.955 ± 0.002	0.314 ± 0.002	3	0.160 ± 0.007	0.750 ± 0.005	0.01/(4)
	(3.0, 3.5)	(0.48, 0.58)	0.955 ± 0.003	0.315 ± 0.003	3	0.660 ± 0.030	0.752 ± 0.008	0.01/(1)
	(3.5, 4.0)	(0.48, 0.58)	0.955 ± 0.005	0.193 ± 0.004	5	0.165 ± 0.005	0.768 ± 0.016	2/(3)
	(4.0, 4.6)	(0.48, 0.58)	0.955 ± 0.004	0.195 ± 0.005	5	0.280 ± 0.010	0.776 ± 0.020	0.01/(1)
$\gamma^*p \rightarrow \rho^0 p$	(1.6, 1.9)	(0.16, 0.22)	0.960 ± 0.005	0.112 ± 0.001	3	1.200 ± 0.060	0.274 ± 0.003	4/11
	(1.6, 1.9)	(0.22, 0.28)	0.960 ± 0.004	0.115 ± 0.001	3	2.300 ± 0.090	0.282 ± 0.002	2/10
	(1.9, 2.2)	(0.22, 0.28)	0.960 ± 0.003	0.119 ± 0.002	3	1.200 ± 0.050	0.291 ± 0.005	1/11
	(2.2, 2.5)	(0.22, 0.28)	0.960 ± 0.003	0.120 ± 0.001	3	1.000 ± 0.030	0.294 ± 0.003	2/11
	(1.6, 1.9)	(0.28, 0.34)	0.960 ± 0.005	0.119 ± 0.004	3	6.100 ± 0.210	0.291 ± 0.010	8/10
	(1.9, 2.2)	(0.28, 0.34)	0.960 ± 0.007	0.121 ± 0.004	3	2.200 ± 0.080	0.296 ± 0.010	5/11
	(2.2, 2.5)	(0.28, 0.34)	0.960 ± 0.003	0.126 ± 0.003	3	1.400 ± 0.040	0.309 ± 0.008	4/11
	(2.5, 2.8)	(0.28, 0.34)	0.960 ± 0.010	0.127 ± 0.004	3	1.000 ± 0.030	0.311 ± 0.010	2/11
	(1.9, 2.2)	(0.34, 0.40)	0.960 ± 0.004	0.163 ± 0.005	3	4.000 ± 0.170	0.399 ± 0.012	7/11
	(2.2, 2.5)	(0.34, 0.40)	0.960 ± 0.020	0.168 ± 0.014	3	1.700 ± 0.090	0.412 ± 0.034	3/11
	(2.5, 2.8)	(0.34, 0.40)	0.960 ± 0.016	0.175 ± 0.005	3	1.250 ± 0.070	0.429 ± 0.013	2/11
	(2.8, 3.1)	(0.34, 0.40)	0.960 ± 0.006	0.177 ± 0.003	3	1.000 ± 0.080	0.434 ± 0.008	2/11
	(3.1, 3.6)	(0.34, 0.40)	0.960 ± 0.004	0.178 ± 0.002	3	0.700 ± 0.030	0.436 ± 0.005	2/11
	(2.2, 2.5)	(0.40, 0.46)	0.960 ± 0.020	0.185 ± 0.010	3	3.300 ± 0.160	0.453 ± 0.024	9/11
	(2.5, 2.8)	(0.40, 0.46)	0.960 ± 0.008	0.190 ± 0.006	3	2.100 ± 0.140	0.465 ± 0.014	4/11
	(2.8, 3.1)	(0.40, 0.46)	0.960 ± 0.020	0.215 ± 0.008	3	1.300 ± 0.090	0.527 ± 0.020	0.4/11
	(3.1, 3.6)	(0.40, 0.46)	0.960 ± 0.010	0.217 ± 0.006	3	0.800 ± 0.060	0.532 ± 0.015	0.7/11
	(3.6, 4.1)	(0.40, 0.46)	0.960 ± 0.015	0.218 ± 0.020	3	0.700 ± 0.040	0.534 ± 0.049	2/11
	(2.8, 3.1)	(0.46, 0.52)	0.960 ± 0.020	0.250 ± 0.010	3	2.000 ± 0.150	0.612 ± 0.025	8/11
	(3.1, 3.6)	(0.46, 0.52)	0.960 ± 0.002	0.254 ± 0.002	3	0.900 ± 0.060	0.622 ± 0.005	1/11
	(3.6, 4.1)	(0.46, 0.52)	0.960 ± 0.010	0.270 ± 0.006	3	0.800 ± 0.050	0.661 ± 0.015	1/11
	(4.1, 4.6)	(0.46, 0.52)	0.960 ± 0.009	0.272 ± 0.002	3	0.800 ± 0.030	0.666 ± 0.005	2/11
	(3.6, 4.1)	(0.52, 0.58)	0.960 ± 0.020	0.300 ± 0.020	3	1.200 ± 0.070	0.735 ± 0.049	6/11
	(4.1, 4.6)	(0.52, 0.58)	0.960 ± 0.020	0.400 ± 0.030	3	1.000 ± 0.050	0.980 ± 0.073	1/10
	(4.1, 4.6)	(0.58, 0.64)	0.960 ± 0.020	0.410 ± 0.030	3	1.000 ± 0.040	1.004 ± 0.074	6/10
	(4.6, 5.1)	(0.58, 0.64)	0.960 ± 0.010	0.420 ± 0.020	3	0.900 ± 0.030	1.029 ± 0.049	6/10
	(5.1, 5.6)	(0.64, 0.70)	0.960 ± 0.010	0.430 ± 0.010	3	0.900 ± 0.040	1.053 ± 0.025	0.4/(4)

In addition, x_B also represents the longitudinal momentum fraction transferred to the struck parton. In the considered $\gamma^*p \rightarrow$ meson + nucleon process in ep collisions at given energy, the larger x_B means the larger longitudinal momentum transfer to the struck parton or the system, and hence the more energy deposited to the system. The system naturally stays at higher excitation degree. As a result, larger $\langle p_T \rangle$ and T_i are observed.

Generally, $\langle p_T \rangle > T_i \geq T_{ch} \geq T_0$. If the evolution time of the system is 0, that is if the initial-state, chemical freeze-out, and kinetic freeze-out happen simultaneously, we have $T_i = T_{ch} = T_0$. If the evolution time is not negligible, we have $T_i > T_{ch} > T_0$. The difference between $\langle p_T \rangle$ and temperature is explained as the contribution of flow effect. According to ref. [55], in the final-state, the expected real $T_0 \approx \langle p_T \rangle / 3.07$. Then, we have the contribution of flow effect to be $\langle p_T \rangle - T_0 \approx 2.07 \langle p_T \rangle / 3.07$. One can see that the flow effect contributes largely to $\langle p_T \rangle$. It is expected that the contribution of flow effect increases with the increase of evolution time, if $\langle p_T \rangle$ is fixed from the initial- to final-states.

From Tables 1 and 2, we note that the values of n_s are 3–5 for different channels. As the number of participant partons, n_s is constrained to be integer with uncertainty of 0. For a given channel, n_s is independent of Q^2 and x_B in most cases. The channel independent n_s renders that the number of participant partons is not too small or big. The number of struck parton(s) is usually regarded as 1 or 2, which is very small. The struck parton(s) and the partons around the struck parton(s) are participant partons. The partons far away from the struck parton(s) are remainder or spectator partons.

Before summary and conclusions, we would like to point out that the discussion about the temperature and flow in this paper is applicable. Although the multiplicity in ep collisions at a few GeV is very limited and the final particles are in a state far from thermal equilibrium, we may use the grand canonical ensemble for lots of events in which the number of total particles is very large and the whole system is in a homogeneous and equilibrium state. Therefore, the temperature used in this paper is comparable to the freeze-out temperatures used in nucleus-nucleus collisions. Of course, we may also regard the temperature used here as a fitting parameter if necessary.

The initial-temperature T_i is extracted from the root-mean-square of p_T , which is independent of model, though the relation between T_i and $\sqrt{\langle p_T^2 \rangle}$ is from the color string percolation method [43–46]. As deep inelastic scattering, ep collisions are head-on collisions, and may be harder than nucleus-nucleus collisions at similar

energy per nucleon due to the fact that some non-head-on nucleon-nucleon collisions exist in the later. As a hybrid state of head-on and non-head-on nucleon-nucleon collisions, nucleus-nucleus collisions may be weaker than head-on ep collisions. In addition, cold spectator nuclear effect also causes the temperature in nucleus-nucleus collisions to reduce. This renders that T_i obtained in this paper is higher than that in nucleus-nucleus collisions.

It should be emphasized that the parameter T_i reflects the violent degree of collisions. To our knowledge, other groups and other studies where T_i is extracted for hadronic collisions is not available at present, though T_i for nucleus-nucleus collisions is available. In terms of T_i , Erlang distribution, and Monte Carlo calculation, the present work has proposed an alternative method to describe light meson electroproduction data obtained with the JLab-CLAS facility. Typically those data are interpreted in terms of handbag diagram within the formalism of generalized parton distributions, whereas here statistical methods, that were developed for high-energy nucleus-nucleus collisions, are applied. At least, the present work has significance in the application of statistical methods.

IV. SUMMARY AND CONCLUSIONS

In summary, the squared momentum transfer spectra of π^0 , π^+ , η , and ρ^0 produced in $\gamma^*p \rightarrow$ meson + nucleon process have been fitted by the calculated results with the Erlang distribution which is obtained from the multi-source thermal model and used to describe the transverse momentum spectra of emitted particles. The squared momentum transfer undergoes from the incident γ^* to emitted meson, and also equivalently from the target proton to emitted nucleon. The model results are in agreement with the experimental data measured by the CLAS Collaboration. The values of the related parameters are extracted in the fitting process. The squared photon virtuality Q^2 and Bjorken variable x_B dependent parameters are obtained.

With increasing of Q^2 , the quantities $\langle p_T \rangle$ and T_i increase generally. Q^2 is defined as absolute value of the squared mass of the virtual photon that is exchanged between the electron and the target proton, and it effectively represents the transverse size of the probe. Q^2 also reflects the hard scale of collisions. A harder scale results in a higher excitation degree of the system, and a larger $\langle p_T \rangle$ and T_i . At harder scale (larger Q^2), the degree of equilibrium decreases because of more disturbance to the

equilibrated residual partons in target particle, though the system is at the state of high degree of excitation.

Similar to the tendency of Q^2 , with an increase of x_B , the quantities $\langle p_T \rangle$ and T_i increase. In the considered $\gamma^*p \rightarrow \text{meson} + \text{nucleon}$ process, x_B represents the longitudinal momentum fraction transferred to the struck parton. The larger x_B means the larger longitudinal momentum transfer to the system. It is natural that $\langle p_T \rangle$ and T_i are larger at larger x_B . In addition, because $x_B \propto Q$, one may argue that x_B also represents the hard scale of collisions. Indeed, it is understandable that larger $\langle p_T \rangle$ and T_i appear at higher x_B .

Data Availability Statement

The data used to support the findings of this study are included within the article and are cited at relevant places within the text as references.

Author Contributions

All authors listed have made a substantial, direct, and intellectual contribution to the work and approved it for publication.

Ethical Approval

The authors declare that they are in compliance with ethical standards regarding the content of this paper.

Disclosure

The funding agencies have no role in the design of the study; in the collection, analysis, or interpretation of the data; in the writing of the manuscript; or in the decision to publish the results.

Funding

The work of Q.W. and F.H.L. was supported by the National Natural Science Foundation of China under Grant Nos. 12047571, 11575103, and 11947418, the Scientific and Technological Innovation Programs of Higher Education Institutions in Shanxi (STIP) under Grant No. 201802017, the Shanxi Provincial Natural Science Foundation under Grant No. 201901D111043, and the Fund for Shanxi “1331 Project” Key Subjects Construction. The work of K.K.O. was supported by the Ministry of Innovative Development of the Republic of Uzbekistan within the fundamental project No. F3-20200929146 on analysis of open data on heavy-ion collisions at RHIC and LHC.

Conflicts of Interest

The authors declare that there are no conflicts of interest regarding the publication of this paper.

-
- [1] Wang H, Chen JH, Ma YG, Zhang S. Charm hadron azimuthal angular correlations in Au+Au collisions at $\sqrt{s_{NN}} = 200$ GeV from parton scatterings. *Nucl Sci Tech* (2019) 30:185. doi:10.1007/s41365-019-0706-z
- [2] Yan TZ, Li S, Wang YN, Xie F, Yan TF. Yield ratios and directed flows of light particles from proton-rich nuclei-induced collisions. *Nucl Sci Tech* (2019) 30:15. doi:10.1007/s41365-018-0534-6
- [3] Fisli M, Mebarki N. Top quark pair-production in non-commutative standard model. *Adv High Energy Phys* (2020) 2020:7279627. doi:10.1155/2020/7279627
- [4] He XW, Wu FM, Wei HR, Hong BH. Energy-dependent chemical potentials of light hadrons and quarks based on transverse momentum spectra and yield ratios of negative to positive particles. *Adv High Energy Phys* (2020) 2020:1265090. doi:10.1155/2020/1265090
- [5] Waqas M, Li BC. Kinetic freeze-out temperature and transverse flow velocity in Au-Au collisions at RHICBES energies. *Adv High Energy Phys* (2020) 2020:1787183. doi:10.1155/2020/1787183
- [6] Tang ZB, Zha WM, Zhang YF. An experimental review of open heavy flavor and quarkonium production at RHIC. *Nucl Sci Tech* (2020) 31:81. doi:10.1007/s41365-020-00785-8
- [7] Shen C, Yan L. Recent development of hydrodynamic modeling in heavy-ion collisions. *Nucl Sci Tech* (2020) 31:122. doi:10.1007/s41365-020-00829-z
- [8] Yu H, Fang DQ, Ma YG. Investigation of the symmetry energy of nuclear matter using isospin-dependent quantum molecular dynamics. *Nucl Sci Tech* (2020) 31:61. doi:10.1007/s41365-020-00766-x
- [9] Bhaduri S, Bhaduri A, Ghosh D. Study of di-muon production process in pp collision in CMS data from symmetry scaling perspective. *Adv High Energy Phys* (2020) 2020:4510897. doi:10.1155/2020/4510897
- [10] Tawfik AN. Out-of-equilibrium transverse momentum spectra of pions at LHC energies. *Adv High Energy Phys* (2020) 2020:4604608. doi:10.1155/2019/4604608
- [11] Nayak JK, Alam J, Sarkar S, Sinha B. Measuring initial temperature through a photon to dilepton ratio in heavy-ion collisions. *J Phys G* (2008) 35:104161. doi:10.1088/0954-3899/35/10/104161

- [12] Adare A, Afanasiev S, Aidala C, Ajitanand NN, Akiba Y, Al-Bataineh H, et al. [PHENIX Collaboration]. Enhanced production of direct photons in Au+Au collisions at $\sqrt{s} = 200$ GeV and implications for the initial temperature. *Phys Rev Lett* (2010) 104:132301. doi:10.1103/PhysRevLett.104.132301
- [13] Csanád M, Májér I. Initial temperature and EoS of quark matter via direct photons. *Phys Part Nucl Lett* (2011) 8:1013. doi:10.1134/S1547477111090147
- [14] Csanád M, Májér I. Equation of state and initial temperature of quark gluon plasma at RHIC. *Cent Eur J Phys* (2012) 10:850. doi:10.2478/s11534-012-0060-9
- [15] Soltz RA, Garishvili I, Cheng M, Abelev B, Glenn A, Newby J, et al. Constraining the initial temperature and shear viscosity in a hybrid hydrodynamic model of $\sqrt{s} = 200$ GeV Au+Au collisions using pion spectra, elliptic flow, and femtoscopic radii. *Phys Rev C* (2013) 87:044901. doi:10.1103/PhysRevC.87.044901
- [16] Waqas M, Liu FH. Initial, effective, and kinetic freeze-out temperatures from transverse momentum spectra in high energy proton(deuteron)-nucleus and nucleus-nucleus collisions. *Eur Phys J Plus* (2020) 135:147. doi:10.1140/epjp/s13360-020-00213-1
- [17] Cleymans J, Paradza MW. Tsallis statistics in high energy physics: chemical and thermal freeze-outs. *Physics* (2020) 2:654. doi:10.3390/physics2040038
- [18] Li LL, Liu FH. Kinetic freeze-out properties from transverse momentum spectra of pions in high energy proton-proton collisions. *Physics* (2020) 2:277. doi:10.3390/physics2020015
- [19] Wang Q, Liu FH, Olimov KK. Initial and final-state temperatures of emission source from differential cross-section in squared momentum transfer in high energy collisions. *Adv High Energy Phys* (2021) 2021:6677885. doi:10.1155/2021/6677885
- [20] Liu FH, Li JS. Isotopic production cross section of fragments in $^{56}\text{Fe}+p$ and $^{136}\text{Xe}(^{124}\text{Xe})+\text{Pb}$ reactions over an energy range from 300A to 1500A MeV. *Phys Rev C* (2008) 78:044602. doi:10.1103/PhysRevC.78.044602
- [21] Liu FH. Unified description of multiplicity distributions of final-state particles produced in collisions at high energies. *Nucl Phys A* (2008) 810:159. doi:10.1016/j.nuclphysa.2008.06.014
- [22] Liu FH, Gao YQ, Tian T, Li BC. Unified description of transverse momentum spectrums contributed by soft and hard processes in high-energy nuclear collisions. *Eur Phys J A* (2014) 50:94. doi:10.1140/epja/i2014-14094-9
- [23] Tsallis C. Possible generalization of Boltzmann-Gibbs statistics. *J Stat Phys* (1988) 52:479. doi:10.1007/BF01016429
- [24] Abelev BI, Adams J, Aggarwal MM, Ahammed Z, Amonett J, Anderson BD, et al. [STAR Collaboration]. Strange particle production in $p + p$ collisions at $\sqrt{s} = 200$ GeV. *Phys Rev C* (2007) 75:064901. doi:10.1103/PhysRevC.75.064901
- [25] Hagedorn R. Multiplicities, p_T distributions and the expected hadron \rightarrow quark-gluon phase transition. *Riv Nuovo Cim* (1983) 6(no.10):1. doi:10.1007/BF02740917
- [26] Zhang NS. Particle Physics (Volume I), Science Press, Beijing, China (1986) p. 116
- [27] Sarkisyan EKG, Sakharov AS. Multihadron production features in different reactions. *AIP Conf Proc* (2006) 828:35. doi:10.1063/1.2197392
- [28] Sarkisyan EKG, Sakharov AS. Relating multihadron production in hadronic and nuclear collisions. *Eur Phys J C* (2010) 70:533. <https://doi.org/10.1140/epjc/s10052-010-1493-1>
- [29] Mishra AN, Sahoo R, Sarkisyan EKG, Sakharov AS. Effective-energy budget in multiparticle production in nuclear collisions. *Eur Phys J C* (2014) 74:3147. doi:10.1140/epjc/s10052-014-3147-1
- [30] Sarkisyan EKG, Mishra AN, Sahoo R, Sakharov AS. Multihadron production dynamics exploring the energy balance in hadronic and nuclear collisions. *Phys Rev D* (2016) 93:054046. doi:10.1103/PhysRevD.93.054046
- [31] Sarkisyan EKG, Mishra AN, Sahoo R, Sakharov AS. Centrality dependence of midrapidity density from GeV to TeV heavy-ion collisions in the effectiveenergy universality picture of hadroproduction. *Phys Rev D* (2016) 94:011501(R). doi:10.1103/PhysRevD.94.011501
- [32] Sarkisyan EKG, Mishra AN, Sahoo R, Sakharov AS. Effective-energy universality approach describing total multiplicity centrality dependence in heavy-ion collisions. *Eurphys Lett* (2019) 127:62001. doi:10.1209/0295-5075/127/62001
- [33] Mishra AN, Ortiz A, Paić G. Intriguing similarities of high- p_T particle production between pp and $A - A$ collisions. *Phys Rev C* (2019) 99:034911. doi:10.1103/PhysRevC.99.034911
- [34] Castorina P, Plumari S, Satz H. Universal strangeness production in hadronic and nuclear collisions. *Int J Mod Phys E* (2016) 25:1650058. doi:10.1142/S0218301316500580
- [35] Castorina P, Plumari S, Satz H. Universality in high energy collisions of small and large systems. Proceedings of the 40th International Conference on High Energy Physics – ICHEP2020, July 28 – August 6, 2020, Prague, Czech Republic (virtual meeting). *Proceedings of Science* (2020) 390(ICHEP2020):537. doi:10.22323/1.390.0537
- [36] Castorina P, Plumari S, Satz H. Universality in hadronic and nuclear collisions at high energy. *Phys Rev C* (2020) 101:054902. doi:10.1103/PhysRevC.101.054902
- [37] Bedlinskiy I, Kubarovskiy V, Niccolai S, Stoler P, Adhikari KP, Anderson MD, et al. [CLAS Collaboration]. Exclusive π^0 electroproduction at $W >$

- 2 GeV with CLAS. *Phys Rev C* (2014) 90:025205. doi:10.1103/PhysRevC.90.025205
- [38] Park K, Guidal M, Gothe RW, Laget JM, Garçon M, Adhikari KP, et al. [CLAS Collaboration]. Deep exclusive π^+ electroproduction off the proton at CLAS. *Eur Phys J A* (2013) 49:1. doi:10.1140/epja/i2013-13016-9
- [39] Bedlinskiy I, Kubarovsky V, Stoler P, Adhikari KP, Akbar Z, Pereira SA, et al. [CLAS Collaboration]. Exclusive η electroproduction at $W > 2$ GeV with CLAS and transversity generalized parton distributions. *Phys Rev C* (2017) 95:035202. doi:10.1103/PhysRevC.95.035202
- [40] Morrow SA, Guidal M, Garçon M, Laget JM, Smith ES, Adams G, et al. [CLAS Collaboration]. Exclusive ρ^0 electroproduction on the proton at CLAS. *Eur Phys J A* (2009) 39:5. doi:10.1140/epja/i2008-10683-5
- [41] An CS, Saghai B. Sea-quark flavor content of octet baryons and intrinsic five-quark Fock states. *Phys Rev C* (2012) 85:055203. doi:10.1103/PhysRevC.85.055203
- [42] An CS, Saghai B. Strangeness magnetic form factor of the proton in the extended chiral quark model. *Phys Rev C* (2013) 88:025206. doi:10.1103/PhysRevC.88.025206
- [43] Gutay LG, Hirsch AS, Pajares C, Scharenberg RP, Srivastava BK. De-confinement in small systems: clustering of color sources in high multiplicity $\bar{p}p$ collisions at $\sqrt{s} = 1.8$ TeV. *Int J Mod Phys E* (2015) 24:1550101. doi:10.1142/S0218301315501013
- [44] Scharenberg RP, Srivastava BK, Pajares C. Exploring the initial stage of high multiplicity proton-proton collisions by determining the initial temperature of the quark-gluon plasma. *Phys Rev D* (2019) 100:114040. doi:10.1103/PhysRevD.100.114040
- [45] Sahoo P, De S, Tiwari SK, Sahoo R. Energy and centrality dependent study of deconfinement phase transition in a color string percolation approach at RHIC energies. *Eur Phys J A* (2018) 54:136. doi:10.1140/epja/i2018-12571-9
- [46] Wang Q, Liu FH. Excitation function of initial temperature of heavy flavor quarkonium emission source in high energy collisions. *Adv High Energy Phys* (2020) 2020:5031494. doi:10.1155/2020/5031494
- [47] Aaron FD, Martin MA, Alexa C, Andreev V, Antunovic B, Asmone A, et al. [H1 Collaboration]. Diffractive electroproduction of ρ and ϕ mesons at HERA. *J High Energy Phys* (2010) 2010(no. 05):32. doi:10.1007/JHEP05(2010)032
- [48] Aktas A, Andreev V, Anthonis T, Antunovic B, Aplin S, Asmone A, et al. [H1 Collaboration]. Elastic J/ψ production at HERA. *Eur Phys J C* (2006) 46:585. doi:10.1140/epjc/s2006-02519-5
- [49] Chekanov S, Derrick M, Magill S, Musgrave B, Nicholass D, Repond J, et al. [ZEUS Collaboration]. Exclusive ρ^0 production in deep inelastic scattering at HERA. *PMC Phys A* (2007) 1:6. doi:10.1186/1754-0410-1-6
- [50] Derrick M, Krakauer D, Magill S, Mikunas D, Musgrave B, Okrasiński JR, et al. [ZEUS Collaboration]. Measurement of elastic ω photoproduction at HERA ZEUS Collaboration. *Z Phys C* (1997) 73:73. doi:10.1007/s002880050297
- [51] Chekanov S, Derrick M, Magill S, Miglioranza S, Musgrave B, Repond J, et al. [ZEUS Collaboration]. Exclusive electroproduction of ϕ mesons at HERA. *Nucl Phys B* (2005) 718:3. doi:10.1016/j.nuclphysb.2005.04.009
- [52] Chekanov S, Derrick M, Loizides JH, Magill S, Miglioranza S, Musgrave B, et al. [ZEUS Collaboration]. Exclusive electroproduction of J/ψ mesons at HERA. *Nucl Phys B* (2004), 695:3. doi:10.1016/j.nuclphysb.2004.06.034
- [53] Barberis D, Binon FG, Close FE, Danielsen KM, Donskov BC, Earl BC, et al. [WA102 Collaboration]. A coupled channel analysis of the centrally produced K^+K^- and $\pi^+\pi^-$ final states in pp interactions at 450 GeV/c. *Phys Lett B* (1999) 462:462. doi:10.1016/S0370-2693(99)00909-0
- [54] Barberis D, Beusch W, Binon FG, Blick AM, Close FE, Danielsen KM, et al. [WA102 Collaboration]. A measurement of the branching fractions of the $f_1(1285)$ and $f_1(1420)$ produced in central pp interactions at 450 GeV/c. *Phys Lett B* (1998) 440:225. doi:10.1016/S0370-2693(98)01264-7
- [55] Giacalone G. A matter of shape: seeing the deformation of atomic nuclei at high-energy colliders. Ph.D. Thesis, Université Paris-Saclay, France. (2021) p. 50. arXiv:2101.00168 (2021)